Structure and basic magnetic properties of the honeycomb lattice compounds $Na_2Co_2TeO_6$ and $Na_3Co_2SbO_6$

L. Viciu[a,*], Q. Huang[b], E. Morosan[a], H.W. Zandbergen[c], N.I. Greenbaum[a], T. McQueen[a], R.J. Cava[a]

[a]*Department of Chemistry, Princeton University, Princeton NJ 08544, USA*
[b]*NIST Center for Neutron Research, NIST, Gaithersburg, MD 20899, USA*
[c]*National Centre for HREM, Department of Nanoscience, Delft Institute of Technology, Al Delft, The Netherlands*

Abstract

The synthesis, structure, and basic magnetic properties of $Na_2Co_2TeO_6$ and $Na_3Co_2SbO_6$ are reported. The crystal structures were determined by neutron powder diffraction. $Na_2Co_2TeO_6$ has a two-layer hexagonal structure (space group $P6_322$) while $Na_3Co_2SbO_6$ has a single-layer monoclinic structure (space group $C2/m$). The Co, Te, and Sb ions are in octahedral coordination, and the edge sharing octahedra form planes interleaved by sodium ions. Both compounds have full ordering of the Co^{2+} and Te^{6+}/Sb^{5+} ions in the *ab* plane such that the Co^{2+} ions form a honeycomb array. The stacking of the honeycomb arrays differ in the two compounds. Both $Na_2Co_2TeO_6$ and $Na_3Co_2SbO_6$ display magnetic ordering at low temperatures, with what appears to be a spin-flop transition found in $Na_3Co_2SbO_6$.
© 2007 Published by Elsevier Inc.

1. Introduction

The study of the magnetic properties of low dimensional systems has played an important role in condensed matter physics [1]. The understanding of both the theoretical models and the concepts of low dimensional magnets gained momentum with the discovery of high T_c superconductivity in cuprates, where the magnetic ions are arranged in square planes [2]. Also of recent interest have been triangle-based geometries: when populated with antiferromagnetically coupled magnetic atoms, frustration of the low temperature magnetic states can occur due to conflicting near neighbor spin interactions [3]. In this category, Na_xCoO_2 represents one of the richest systems of current interest [4–8]. The layered structures of the Na_xCoO_2 phases consist of planes of edge-sharing cobalt–oxygen octahedra interleaved with Na ions [9]. The Co ions have a triangular planar lattice, considered an important factor in driving the properties in these phases.

One variant of the triangular lattice is the honeycomb geometry, where 1/3 of the sites of a triangular lattice are non-magnetic. Compounds with the magnetic ions in this geometry have manifested interesting properties such as spin-glass behavior [10], spin-flop transitions [11] and even superconductivity [12]. Here we report the synthesis, structural and magnetic characterization of two Co-based compounds, $Na_2Co_2TeO_6$ and $Na_3Co_2SbO_6$, in which the Co ions are arranged in a honeycomb lattice. $Na_3Co_2SbO_6$ was recently described as being trigonal [13] but no other information related to the synthesis, structural or physical property characterization of this phase is available. The Te-based compound has not been previously reported.

2. Experimental

$Na_2Co_2TeO_6$ and $Na_3Co_2SbO_6$ were prepared by mixing Na_2CO_3 (Alfa, 99.5%) and Co_3O_4 (Alfa, 99.7%) with TeO_2

---

*Corresponding author. Fax: 609 258 6746.

  E-mail address: mviciu@Princeton.edu (L. Viciu).

(JMC, 99.9995%) or Sb_2O_4 (Sb_2O_5 Alfa, 99.5%, annealed for 12 h at 1000 °C in air to prepare Sb_2O_4). The Co:(Sb,Te) ratio was stoichiometric, but 20% excess Na_2CO_3 was added to compensate for loss due to volatilization. The mixtures were thoroughly ground, pressed into pellets ($\phi = 13$ mm) and annealed under flowing nitrogen as follows: 8 days at 800 °C were necessary for $Na_2Co_2TeO_6$ with two intermediate grindings—one after 4 days and then another one after 2 days of subsequent annealing; $Na_3Co_2SbO_6$ was obtained after 2 days of thermal treatment at 800 °C. In all cases, the furnace temperature was increased by 5 °C/min until the desired temperature was reached. Slow cooling to room temperature after reaction completion, 5 °C/min, was performed. The compounds are both lightly pastel-colored, indicating that they have large band gaps and no significant electrical conductivity or Co mixed valency.

The purity of the samples was analyzed by powder X-ray diffraction using Cu$K\alpha$ radiation and a diffracted beam monochromator. Neutron diffraction data were collected on $Na_2Co_2TeO_6$ and $Na_3Co_2SbO_6$ at the NIST Center for Neutron Research on the high resolution powder neutron diffractometer (BT1) with monochromatic neutrons of wavelength 1.5403 Å produced by a Cu(311) monochromator. Collimators with horizontal divergences of 15′, 20′ and 7′ of arc were used before and after the monochromator and after the sample, respectively. Data were collected in the 2-θ range of 3–168° with a step size of 0.05°. The structural parameters were refined using the program GSAS [14] The sodium content in each sample was determined by the structure refinement, and was in good agreement with that expected from nominal compositions.

The magnetic properties were measured with a Quantum Design PPMS system. Zero field cooled (ZFC) and field cooled (FC) magnetization data were taken between 1.8 and 280 K in an applied field of 1 T. Field dependent magnetization data were recorded at 5 and 30 K for $Na_2Co_2TeO_6$, and at 5, 8 and 12 K for $Na_3Co_2SbO_6$.

3. Results

The purity of the compounds was confirmed by X-ray diffraction analysis. The powder neutron diffraction pattern of $Na_2Co_2TeO_6$ was indexed with a hexagonal cell in the space group $P6_322$ (No.182), while that of $Na_3Co_2SbO_6$ was indexed with a centered monoclinic cell in the space group $C2/m$ (No. 12). Structural analysis by the Rietveld method based on the powder neutron diffraction data was performed for both compounds. The cell constants, as determined by powder neutron diffraction, are presented in Tables 1 and 2. $Na_2Co_2TeO_6$ displays a primitive, two-layer hexagonal structure, while $Na_3Co_2SbO_6$ has a single layer monoclinic structure, very similar to what is seen in $Na_3Cu_2SbO_6$ [13].

The neutron powder diffraction pattern for $Na_2Co_2TeO_6$ shows it to have no observable dimensional deviations from hexagonal symmetry. Its honeycomb-based crystal structure was found to be very well described in space group $P6_322$. A classic two-layer structure, similar to that of $Na_{0.7}CoO_2$ [9], but with a larger in-plane unit cell to accommodate the honeycomb-type cobalt-tellurium ordering, is found. The crystal structure is presented in Figs. 3a and b. Two symmetry-independent Co ions within the honeycomb layer, one type of Te, one type of oxygen, and three independent Na ion positions were found. Models in which Co–Te intermixing was tested for the metal atom sites did not yield significant mixing: the atoms are fully ordered. Refinements were carried out with atoms of the same type constrained to have the same thermal parameters.

The Na distribution between the honeycomb layers is highly disordered. The geometry of the oxygen array in the planes neighboring the Na planes creates triangular prismatic sites for the Na, exactly as is found in two-layer Na_xCoO_2. In the Na_xCoO_2 structures, Na is found to occupy triangular prisms of two types: one type that shares only edges with the metal octahedra in the planes above and below, and one that shares faces with the metal octahedra in the planes above and below. The same situation is found for $Na_2Co_2TeO_6$. In this case, though, there are two types of face sharing possible, as the triangular prisms can share faces with one Co octahedron and one Te octahedron in the planes above and below, or with two Co octahedra. The final refinements (Table 1) showed that the Na ions partially occupy all three types of available triangular prismatic sites, in different amounts: 71% of the Na are in the triangular prisms that share edges

Table 1
Crystallographic data for $Na_2Co_2TeO_6$ in the space group $P6_322$ (no. 182), $a = 5.2889(1)$ Å, $c = 11.2149(4)$ Å, volume $= 271.68(1)$ Å^3

Atom	Wyckoff position	x	y	z	$U_{iso} \times 100$ (Å)	Occ.
Co(1)	2b	0	0	1/4	0.8(1)	1
Co(2)	2d	2/3	1/3	1/4	0.8(1)	1
Te	2c	1/3	2/3	1/4	0.9(1)	1
O	12i	0.6432(6)	−0.0252(4)	0.3452(1)	1.50(4)	1
Na(1)	12i	0.24(1)	0.65(2)	−0.026(3)	0.8(3)	0.081(7)
Na(2)	2a	0	0	0	0.8(3)	0.11(3)
Na(3)	12i	0.702(3)	0.066(2)	−0.006(2)	0.8(3)	0.234(6)

$\chi^2 = 1.39$; w$R_p = 6.53$; $R_p = 5.05$; $R(F^2) = 8.4\%$.

Table 2

Crystallographic data for $Na_3Co_2SbO_6$ in the space group $C2/m$ (no. 12), $a = 5.3681(2)$ Å, $b = 9.2849(4)$ Å, $c = 5.6537(2)$ Å, $\beta = 108.506(4)°$, volume $= 267.22(2)$ Å^3

Atom	Wyckoff position	x	y	z	$U_{iso} \times 100$ (Å^2)	Occ.
Co	4g	0	2/3	0	0.23(12)	1
Sb	2^a	0	0	0	1.86(17)	1
O(1)	8j	0.2744(8)	0.3410(3)	0.7971(5)	1.25(2)	1
O(2)	4i	0.2463(10)	0.5	0.2056(10)	1.25(2)	1
Na(1)	2d	0	0.5	0.5	1.58(5)	1
Na(2)	4h	0.5	0.3296(9)	0.5	1.58(5)	1

$\chi^2 = 1.01$; $wR_p = 5.31\%$; $R_p = 4.31\%$; $R(F^2) = 7.57\%$.

with octahedra in the honeycomb layers, 23% are in the prisms that share faces with the Co and Te, and 6% are in sites that share faces with two Co. The reason for this distribution is not understood, but as in the case of two-layer Na_xCoO_2, the fact that the face sharing positions are occupied at all indicates that the difference in energy that occurs on sharing faces with the octahedra in neighboring planes is not as important as other factors such as Na—Na interactions in determining the Na distribution. Again as in the case of Na_xCoO_2 [15,16], some of the Na ions were found to be displaced towards the faces of their triangular prisms. Refinements in which the Na were left in the centers of their coordination polyhedra resulted in worse agreement factors ($\chi^2 = 1.47$, $wR_P = 6.72$, $R_P = 5.26$) than for the final model, and physically unrealistic thermal vibration parameters for the Na. It was found that displacement of Na(2) did not significantly improve the agreement factors or the thermal vibration parameters, so in the final refinement, only Na(1) and Na(3) were allowed to relax from their ideal positions; they were found to displace towards the faces of the prisms. The freely refined occupancies of the three Na sites, which are all partially occupied, yield a formula within experimental uncertainty of the ideal $Na_2Co_2TeO_6$ composition. The final model provides an excellent fit to the data. The observed, calculated, and difference plots for the refinement based on this model are presented in Fig. 1. The refined structural parameters are presented in Table 1. The Na distribution is shown in Fig. 4.

Selected bond distances are shown in Table 3. The two independent Co sites have very similar Co–O bond distances within their octahedra, 2.11 and 2.13 Å for Co(1) and Co(2), respectively. The $Te^{6+}O_6$ octahedron is significantly smaller (Te–O bond length $= 1.95$ Å), as expected. The bond valence sums are consistent with the assignment of Co^{2+} and Te^{6+} as formal oxidation states. The two-layer stacking sequence found for $Na_2Co_2TeO_6$ is distinctly different from that found for the Cu analog, $Na_2Cu_2TeO_6$ [17], which, though monoclinic, is based on a pseudo-hexagonal three-layer stacking sequence.

$Na_3Co_2SbO_6$ was found to be isostructural with $Na_3Cu_2SbO_6$. It has a single layer structure, well described in the $C2/m$ space group. The structure displays one type of Co, one type of Sb, two independent sodium ions and two
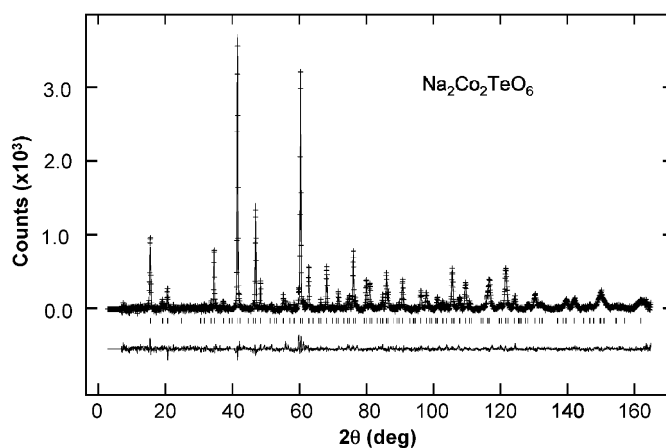

Fig. 1. Observed (crosses) and calculated (solid line) neutron diffraction intensities for $Na_2Co_2TeO_6$ at 295 K. Vertical bars show the Bragg peak positions. Regions in the pattern in the vicinity of two impurity peaks (39.6–40.7° and 59.8–60.1°) were omitted from the refinement. The difference plot is shown at the bottom.

Table 3

Selected bond distances (Å) for $Na_2Co_2TeO_6$ and $Na_3Co_2SbO_6$ at room temperature. BVS = bond valence sum

$Na_2Co_2TeO_6$		$Na_3Co_2SbO_6$	
Co(1)–O × 6	2.112(3)	Co–O(1) × 2	2.132(4)
Co(2)–O × 6	2.131(3)	Co–O(2) × 2	2.124(3)
BVS	1.93 (Co(1))	Co–O(1) × 2	2.125(4)
	1.83 (Co(2))		1.85
Te–O × 6	1.951(2)	Sb–O(1) × 4	2.026(3)
BVS	5.98	Sb–O(2) × 2	2.057(6)
			5.10
Na(1)–O^a	2.50(5)	Na(1)–O(1) × 4	2.367(4)
Na(2)–O	2.515(3)	Na(1)–O(2) × 2	2.427(6)
Na(3)–O^a	2.49(1)	Na(2)–O(1) × 2	2.368(4)
		Na(2)–O(1) × 2	2.431(6)
		Na(2)–O(2) × 2	2.385(6)
Co–Co	3.054 × 3		3.095 × 1
			3.098 × 2

^{a}The bond length is averaged over 6 different bonds.

different oxygen sites. The refinement, using starting positions[9] from $Na_3Cu_2SbO_6$ quickly converged to a final structural model. Refinements were performed in which the Sb and Co occupancies of the sites were allowed to vary. The additional structural parameter did result in a small

improvement in the fit ($\chi^2 = 1.01$ for ordered model vs. 0.99 for a disordered model) but the mixing was not significant. The freely refined Na site occupancies were found to be within experimental uncertainty of full occupancy, yielding the ideal composition. All site occupancies were therefore set to 1 in the final refinements. The final structural parameters are presented in Table 2. The observed, calculated, and difference plots for the neutron diffraction data, using the final model, showing the excellent fit of the model to the data, are presented in Fig. 2. The crystal structure is presented in Fig. 3a and c. Selected bond distances are shown in Table 3. The monoclinic symmetry allows for the possibility of distortion of the Co^{2+}–O octahedron, but the six Co–O distances are in the range of 2.12–2.13 Å, showing that no substantial distortion has occurred. The Co–O bond lengths are very similar to those observed for $Na_2Co_2TeO_6$ (2.11–2.13 Å). The SbO_6 octahedron in $Na_3Co_2SbO_6$ has a size (Sb^{5+}–O distances 2.03–2.06 Å) similar to that found for the Co–O octahedron. The bond valence sums are consistent with the assignment of Co^{2+} and Sb^{5+} as formal oxidation states (Table 3).

Fig. 4 The temperature- and field-dependent magnetization data for $Na_2Co_2TeO_6$ and $Na_3Co_2SbO_6$ are shown in Figs. 5–8. Magnetic ordering transitions are seen near 18 and 4 K, respectively (insets to Figs. 5 and 7). In applied fields of $H = 1$ T, the inverse susceptibilities H/M (open triangles, Figs. 5 and 7) appear to be linear above 150 K, suggesting Curie–Weiss behavior. The temperature range of apparent linear inverse susceptibility is high, however, when compared to the magnetic ordering temperatures. This suggests either that a temperature independent (diamagnetic) contribution to the susceptibility needs to be considered, or that a Heisenberg model for a honeycomb antiferromagnet [18] is a more appropriate description of the M(T) data. For both compounds, the high temperature series expansion (HTSE) for an $S = 3/2$ honeycomb antiferromagnet resulted in slightly poorer fits
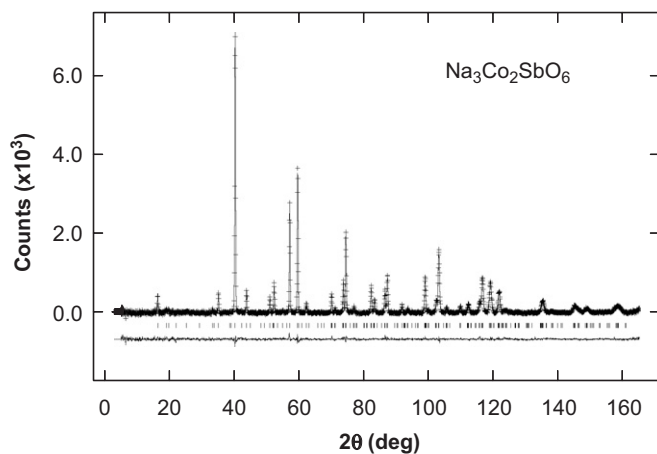
than the Curie–Weiss fits that included a temperature independent diamagnetic contribution to M(T).

After a temperature independent diamagnetic contribution $M_0/H = -2.2 \times 10^{-3}$ emu/mol$_{Co}$ is subtracted from the measured M(T) of $Na_2Co_2TeO_6$, the resulting inverse susceptibility (open squares, Fig. 5) is linear down to approximately 30 K. The effective magnetic moment inferred from the linear fits of the inverse susceptibility data, before and after the diamagnetic corrections were applied, are $\mu_{eff} = 4.97\,\mu_B$ and $5.64\,\mu_B$ per Co, respectively. These moments are within the range of calculated values for Co^{2+}, with the former being much closer to the commonly observed moment of $4.8\,\mu_B$ for Co^{2+} ions in a high spin d^7 configuration [19]. To help distinguish whether the temperature independent diamagnetic contribution should be included in the fits, the temperature derivatives of H/M, d[H/M]/dT, and $H/(M - M_0)$, d[$H/(M-M_0)$]/dT, are plotted as a function of temperature in Fig. 9. For $Na_2Co_2TeO_6$, the plot shows that a temperature independent derivative, and therefore a temperature independent Co moment, is obtained over a wide temperature range after a subtraction of the temperature independent term M_0. For the uncorrected data, however, it is seen that there is actually no region of temperature independent magnetic moment, and that there is therefore no temperature regime, even well above the magnetic ordering temperature, where the Curie–Weiss form without a temperature independent correction is a good description of the data.

At low temperatures, the temperature dependent magnetization data for $Na_2Co_2TeO_6$ show a maximum near 20 K, with a shape characteristic of what is seen for long range antiferromagnetic (AFM) ordering. From the maximum in d($M \times T$)/dT (inset in Fig. 5) a Néel temperature T_N may be determined, as 17.7 K. A second transition near 9 K is also apparent in the derivative data, possibly associated with spin reorientation. Both transition temperatures are marked by vertical arrows in the figure. The negative Weiss temperature $\theta_W = -17.2$ K obtained from the Curie–Weiss fit including the temperature independent term is consistent with the dominance of AFM interactions. The 5 K M(H) isotherm has a slight upward curvature, confirmed by its derivative (Fig. 6), suggesting the possible presence of a broad metamagnetic or spin flop transition in an applied field. The fact that this upward curvature is not present in the 30 K data indicates that, at this temperature, the system is in the paramagnetic state, consistent with the temperature-dependent data and the T_N value of 17.7 K. Detailed understanding of these magnetic transitions will require further study. The related compounds $BaCo_2(AsO_4)_2$ and $BaCo_2(PO_4)_2$, where the Co^{2+} ions are also located on a honeycomb lattice, display helical magnetic ordering in the honeycomb layers, setting in a similar temperature range, and complex temperature/ field phase diagrams [1,20].

The temperature- and field-dependent magnetization data for $Na_3Co_2SbO_6$ are presented in Figs. 7 and 8. ZFC/FC susceptibility data in an applied magnetic field
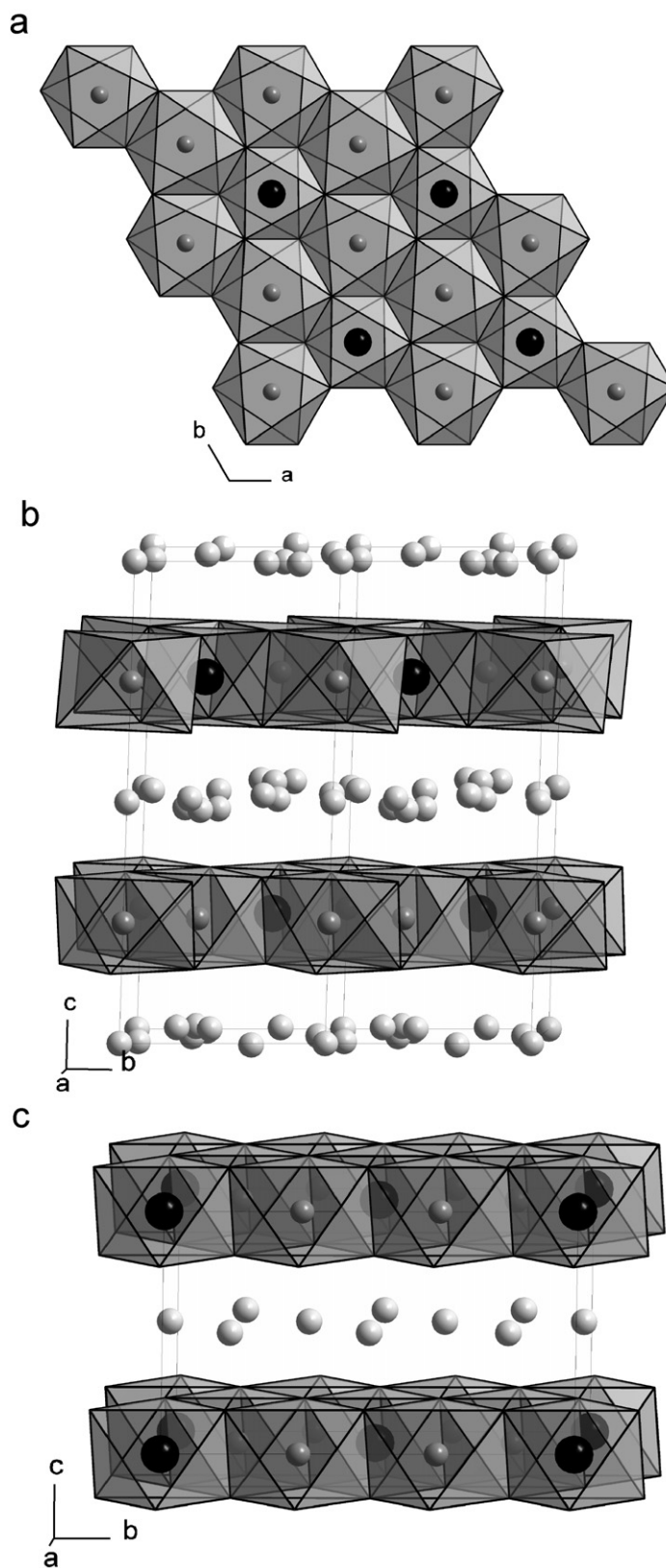

Fig. 2. Observed (crosses) and calculated (solid line) neutron diffraction intensities for $Na_3Co_2SbO_6$ at 295 K. Vertical bars show the Bragg peak positions. The difference plot is shown at the bottom.

Fig. 3. The crystal structures of Na$_2$Co$_2$TeO$_6$ and Na$_3$Co$_2$SbO$_6$: (a) the layer of edge-shared MO$_6$ octahedra, showing the honeycomb Co array; (b) view perpendicular to the honeycomb layers in Na$_2$Co$_2$TeO$_6$; and (c) view perpendicular to the honeycomb layers in Na$_3$Co$_2$SbO$_6$. Inside the octahedra, small dark gray spheres represent Co while bigger black spheres represent Te or Sb. The sodium ions are represented by light gray spheres. Oxygens are at the vertices of the octahedra.
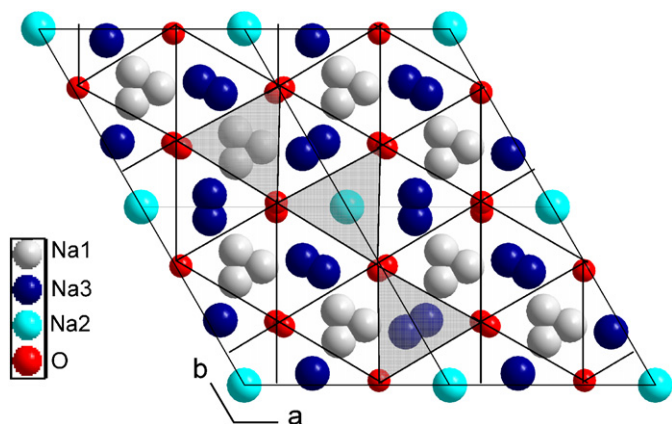
Fig. 4. The Na distribution in $Na_2TeCo_2O_6$. All Na positions are partially occupied. The oxygens in the layers above and below are shown as red spheres. They form three types of triangular prismatic sites for Na. These are marked with their triangular bases in the figure: Na(1) shares faces with one Co and one Te octahedron, and contains approximately 23% of the Na; Na(2) shares faces with two Co octahedra, and contains approximately 6% of the Na; and Na(3) shares only edges with the Co and Te octahedra in the layers above and below and contain approximately 71% of the Na. Na(1) are gray, Na(2) cyan and Na(3) blue spheres, respectively.

Fig. 6. The field dependence at $T = 5$ and 30 K of the magnetization for $Na_2Co_2TeO_6$. The inset shows the magnetization derivative dM/dH vs magnetic field at $T = 5$ and 30 K.

Fig. 5. The temperature dependence for $Na_2Co_2TeO_6$ at $H = 1$ T of the magnetization (left axis) and the inverse susceptibility H/M^* (right axis), where M^* is the measured magnetization M (open triangles) or M—M_0. (open squares). Inset: low-temperature $d(MT)/dT$ at $H = 1$ T.

Fig. 7. The temperature dependence for $Na_2Co_2SbO_6$ at $H = 1$ T of the magnetization (left axis) and the inverse susceptibility H/M^* (right axis), where M^* is the measured magnetization M (open triangles) or M—M_0. (open squares). Inset: low-temperature $d(MT)/dT$ at $H = 1$ T.

$H = 1$ T are indistinguishable and display a maximum below 5 K. This again is suggestive of an AFM transition, with the ordering temperature determined from the maximum in $d(M \times T)/dT$ to be $T_N = 4.4$ K. Similar to the case of $Na_2Co_2TeO_6$, the inverse susceptibility (H/M, open triangles, Fig. 7) appears to be linear above 150 K. After a temperature independent diamagnetic contribution correction $M_0/H = -1.3 \times 10^{-3}$ emu/mol$_{Co}$, the corresponding inverse susceptibility ($H/(M-M_0)$, open squares, Fig. 7) becomes linear only down to ~100 K; the fit using the HTSE model for the honeycomb antiferromagnet was even poorer. The effective magnetic moments determined
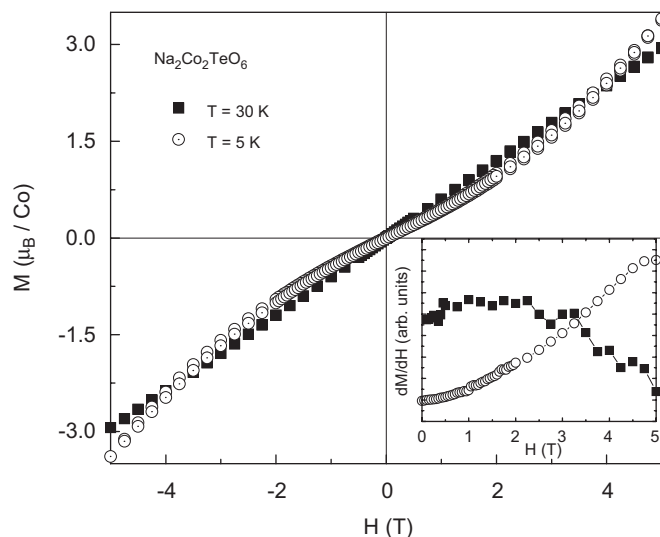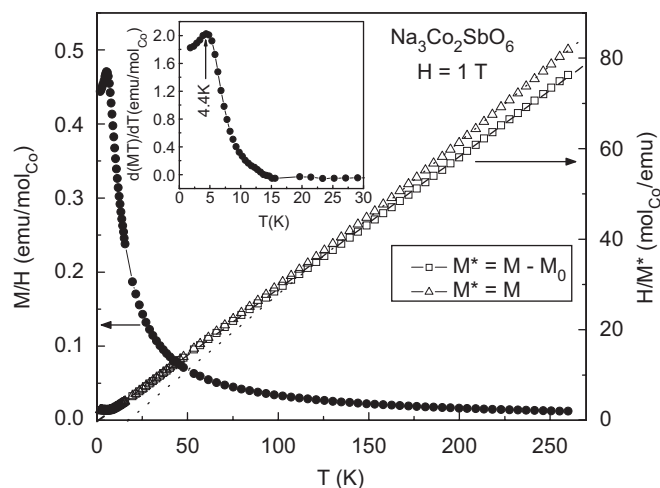
from the linear fits of H/M at high temperatures are 4.90 μ_B and 5.20 μ_B per Co^{2+}, with and without subtracting the diamagnetic contribution M_0. As for the case of $Na_2Co_2TeO_6$, comparison of the temperature derivatives of H/M, $d[H/M]/dT$, and $H/(M-M_0)$, $d[H/(M-M_0)]/dT$, is instructive in determining whether the inclusion of M_0 provides a satisfactory description of the magnetic data (Fig. 9). For $Na_3Co_2SbO_6$ the derivative plot again suggests that the inclusion of an M_0 is a good description for the data, and it also shows that unlike the Te variant, $Na_3Co_2SbO_6$ shows a pre-ordering magnetic effect, possibly from short-range magnetic fluctuations, below approximately 60 K. The Weiss temperature obtained from the Curie–Weiss fit including the temperature independent term in this case is slightly negative, $\theta_W = -0.8$ K
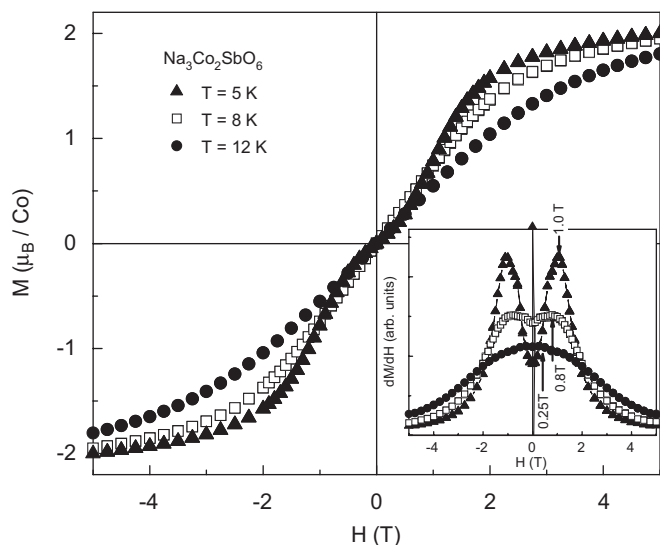
Fig. 8. The field dependence at $T = 5$, 8 and 12 K, of the magnetization for $Na_2Co_2SbO_6$. The inset shows the magnetization derivative dM/dH at $T = 5$, 8 and 12 K. A field-induced transition is clearly seen.
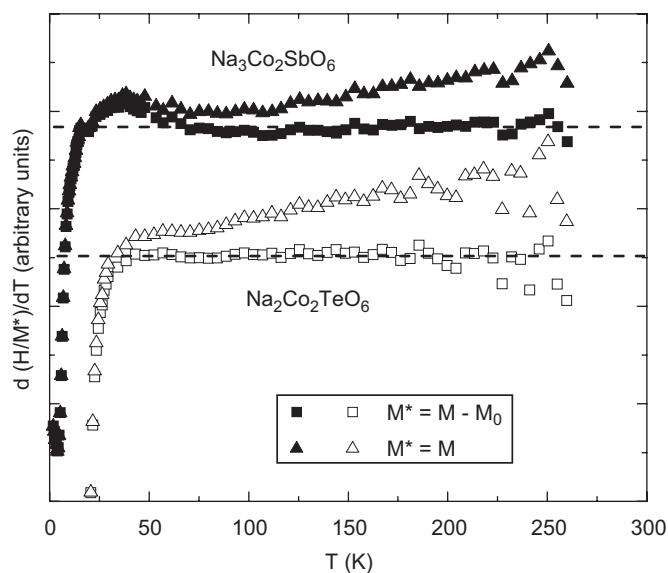

Fig. 9. The temperature dependencies of the temperature derivatives of the inverse susceptibilities for both as-measured H/M, $d[H/M]/dT$, and after a temperature independent correction, $H/(M1M_0)$, $d[H/(M-M_0)]/dT$, for $Na_2Co_2TeO_6$ and $Na_3Co_2SbO_6$. Dashed lines are guides to the eye. $Na_2Co_2TeO_6$ and $Na_3Co_2SbO_6$ data displaced from each other for clarity.

suggesting that AFM interactions are barely dominant. For both materials, ferromagnetic and AFM interactions appear to be very closely balanced, suggesting that there is little to be learned in detail from the Weiss temperatures obtained in the fits.

The $M(H)$ data for $Na_3Co_2SbO_6$ (Fig. 8) show no hysteresis, but indicate the existence of a magnetic field induced transition, with the character of a spin-flop transition, that broadens and moves to lower fields as T increases. The critical field values for the transition are

determined from the maxima in the dM/dH plots shown in the inset. It appears that a field of only 1 T is required to make the Co spins reorient at $T = 5$ K. The $M(H)$ data suggest the existence of an interesting and accessible field-temperature magnetic phase diagram for this compound that may be worthy of further study.

4. Conclusions

The crystal structures of $Na_2Co_2TeO_6$ and $Na_3Co_2SbO_6$ consist of planes of edge-sharing octahedra of CoO_6, TeO_6 and SbO_6 octahedra arranged in an ordered fashion: the magnetic Co^{2+} ions form a honeycomb lattice. In $Na_3Cu_2SbO_6$ and $Na_2Cu_2TeO_6$, due to the Jahn-Teller effect manifested by the Cu ions, the Cu honeycomb lattice is quite distorted, and can be considered a lattice of Cu dimmers [13,15]. No such distortion is found in the Co honeycomb network for either $Na_2Co_2TeO_6$ or
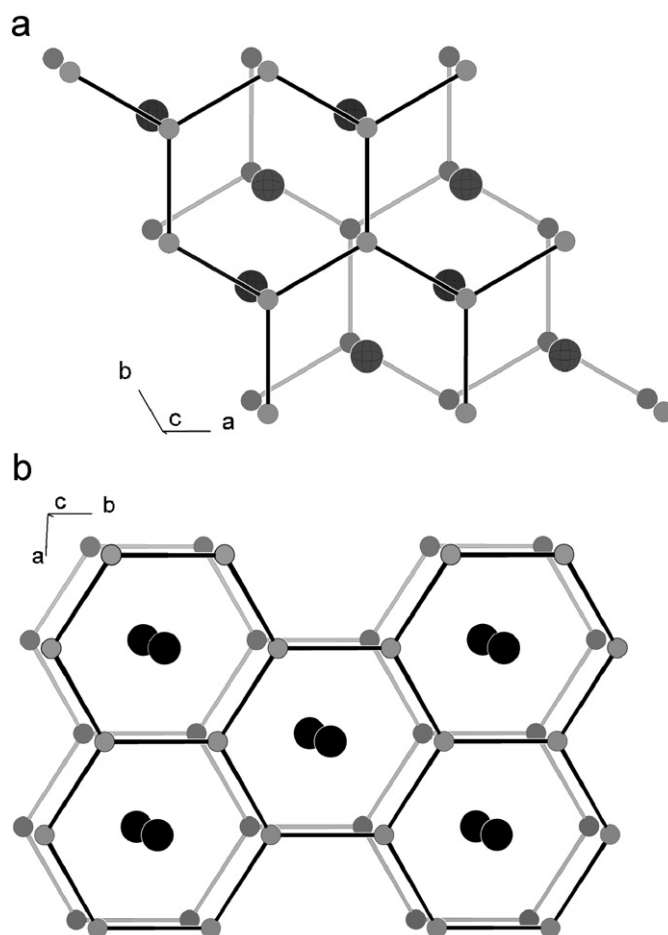

Fig. 10. View of adjacent honeycomb planes in $Na_2Co_2TeO_6$ and $Na_3Co_2SbO_6$, The planes have been tilted slightly so that all the metal atoms are visible: for the Te compound the metals are directly on top of each other in the direction perpendicular to the plane, while in the Sb case they are shifted slightly. For $Na_2Co_2TeO_6$ (a), the stacking of the honeycomb Co lattices in neighboring planes is staggered, while, for (b) $Na_3Co_2SbO_6$, the Co honeycombs stack nearly directly on top of one another. Small dark gray spheres represent Co, bigger black spheres are Sb and big dark gray crossed spheres are Te.

$Na_3Co_2SbO_6$: the honeycomb planes are dimensionally hexagonal in both cases. The most important difference between the structures is the stacking of the honeycomb arrays. In the case of $Na_2Co_2TeO_6$, the Co honeycombs are staggered (Fig. 10a) while in $Na_3Co_2SbO_6$ the Co honeycombs are stacked directly on top of each other (Fig. 10b).

The magnetic susceptibility data for both compounds are consistent with the presence of Co^{2+} ions in the high spin configuration ($S = 3/2$). The in-plane Co–Co distances within the honeycomb for the two compounds are similar, and the in-plane superexchange pathways, through $\sim 90°$ Co–O–Co bonds between edge-sharing octahedra, are also similar. The small negative Weiss temperatures suggest that there is a delicate balance between ferromagnetic and AFM interactions in these compounds. This balance is also manifested in the Co-honeycomb compounds $BaCo_2(AsO_4)_2$ and $BaCo_2(PO_4)_2$, where the magnetic ordering is helical in nature [1,20]. The different magnetic ordering temperatures ($\sim 18\,K$ for the Te compound and $\sim 4\,K$ for the Sb compound), and the difference in behavior in an applied magnetic field, may be due to the difference in honeycomb layer stacking.

$BaCo_2(AsO_4)_2$ and $BaCo_2(PO_4)_2$ are examples of well studied systems in which the Co^{2+} ions are also located on a honeycomb lattice [1,20]. These systems represent classical examples of 2D *XY* magnetic models, and have different, complex magnetic ordering states at low temperatures. Some of the magnetic properties observed for the current compounds, i.e. the field-dependent transitions, are reminiscent of what is seen in those materials. A detailed study of the magnetic behavior of single crystals of $Na_2Co_2TeO_6$ and $Na_3Co_2SbO_6$ would be of particular interest because their honeycomb-based magnetic lattices differ essentially only in stacking: a detailed comparison of their properties may shed light on the effects of interlayer interactions on the low temperature magnetic states of honeycomb lattices.

Acknowledgments

References

[1] L.J. de Jongh, Magnetic Properties of Layered Transition Metal Compounds, Kluwer Academic Publisher, Dordrecht, 1990.
[2] J.G. Bednorz, K.A. Muller, Z. Phys. B 64 (1986) 189.
[3] A.P. Ramirez, Ann. Rev. Mater. Sci. 24 (1994) 453.
[4] M.G.S.R. Thomas, P.G. Bruce, J.B. Goodenough, Solid State Ionics 17 (1985) 13.
[5] I. Terasaki, Y. Sasago, K. Uchinokura, Phys. Rev. B 56 (1997) R12685.
[6] Y.Y. Wang, N.S. Rogado, R.J. Cava, N.P. Ong, Nature 423 (2003) 425.
[7] M.L. Foo, Y. Wang, S. Watauchi, H.W. Zandbergen, T. He, R.J. Cava, N.P. Ong, Phys. Rev. Lett. 92 (2004) 247001.
[8] K. Takada, H. Sakurai, E. Takayama-Muromachi, F. Izumi, R.A. Dilanian, T. Sasaki, Nature 422 (2003) 53.
[9] C. Fouassier, G. Matejka, J.M. Reau, P. Hagenmuller, J. Solid State Chem. 6 (1973) 532.
[10] M. Bieringer, J.E. Greedan, G.M. Luke, Phys. Rev. B 62 (2000) 6521.
[11] D.J. Goossens, A.J. Studer, S.J. Kennedy, T.J. Hicks, J. Phys.: Condens. Matter 12 (2000) 4233.
[12] S. Shamoto, T. Kato, Y. Ono, Y. Miyazaki, K. Ohoyama, M. Ohashi, Y. Yamaguchi, T. Kajitani, Physica C 306 (1998) 7.
[13] O.A. Smirnova, V.B. Nalbandyan, A.A. Petrenko, M. Avdeev, J. Solid State Chem. 178 (2005) 1165.
[14] A. Larson, R.B. Von Dreele, GSAS: Generalized Structure Analysis System, Los Alamos National Laboratory, Los Alamos, NM, 1994.
[15] Q. Huang, M.L. Foo, R.A. Pascal Jr., J.W. Lynn, B.H. Toby, T. He, H.W. Zandbergen, R.J. Cava, Phys. Rev. B 70 (2004) 184110.
[16] J.D. Jorgensen, M. Avdeev, D.G. Hinks, J.C. Burley, S. Short, Phys. Rev. B 68 (2003) 214517.
[17] J. Xu, A. Assoud, N. Soheilnia, S. Derakhshan, H.L. Cuthbert, J.E. Greedan, M.H. Whangbo, H. Kleinke, Inorg. Chem. 44 (2005) 5042.
[18] G.S. Rushbrook, P.J. Wood, Mol. Phys. 1 (1958) 257.
[19] C. Kittel, Introduction in Solid State Physics, 5th ed., Wiley, New York, 1976.
[20] L.P. Regnault, J. Rossat-Mignod, Physica B 86–88 (1977) 660.